PERGAMON

International Journal of Heat and Mass Transfer 42 (1999) 4333–4344

International Journal of HEAT and MASS TRANSFER

www.elsevier.com/locate/ijhmt

Film cooling subject to bulk flow pulsations: effects of blowing ratio, freestream velocity, and pulsation frequency

C.M. Bell, P.M. Ligrani*, W.A. Hull, C.M. Norton

Convective Heat Transfer Laboratory, Department of Mechanical Engineering, University of Utah, Salt Lake City, UT, 84112, USA

Received 17 September 1998; received in revised form 5 March 1999

Abstract

Bulk flow pulsations, in the form of sinusoidal variations of static pressure and streamwise velocity, are investigated as they affect film cooling from round, simple angle holes in a turbulent boundary layer. Such pulsations are important to turbine airfoils and end walls in gas turbine engines because similar pulsations are induced by potential flow interactions and passing families of shock waves. Distributions of adiabatic film cooling effectiveness, iso-energetic Stanton number ratio, and film cooling performance parameter are presented for different pulsation frequencies, blowing ratios, freestream velocities, and hole length-to-diameter ratios. A correlation is given for the onset of protection reduction as it depends upon these parameters. The most important reductions to film cooling protection result as the pulsation frequency increases at the smallest length-to-diameter ratio and smallest blowing ratio tested.

1. Introduction

In recent years, new efforts have been devoted to investigations of the effects of large-scale bulk flow pulsations on film cooling as applied to the turbine surfaces of gas turbine engines [1–15]. This is because of the recognition that passing families of shock waves, potential flow interactions, and passing wakes, which result from the relative motion of adjacent blade rows, can have important detrimental effects on the protection nominally provided by the cooling films. In addition, detailed experimental data illustrating the influences of these phenomena are needed for the design of gas turbine blade components, as well as for the development of more widely applicable numerical models and prediction schemes.

Rigby et al. [1] use an array of rotating bars to simulate nozzle guide vane shock waves and wakes, and examine their effects on an array of turbine blades placed in a linear cascade just downstream. Significant effects of the unsteadiness are apparent on film cooling from two separate rows of holes placed on a blade suction surface. However, the film cooling from holes placed on the pressure surface are only slightly affected by the imposed unsteadiness. In an investigation of rotor heat transfer in a short-duration blow-down turbine test facility, Abhari and Epstein [2] indicate that families of passing shock waves and potential flow interactions cause the time-averaged heat transfer rate to increase by 12% on the suction surface downstream of two rows of holes with blowing ratios from 0.96 to 1.24 (compared with values measured with no pulsations). Increases of 5% are observed on the pressure surface downstream of three rows of holes with blowing ratios from 1.1 to 1.52. Juhany and Hunt [3], Kanda et al. [4], Abhari [5], and Garg and Abhari [6] provide additional data which illustrates the dramatic

* Corresponding author. Tel.: +1-801-581-4240; fax: +1-801-585-9826.

E-mail address: ligrani@mech.utah.edu (P.M. Ligrani)

0017-9310/99/$ - see front matter
PII: S0017-9310(99)00088-5

Nomenclature

C_1	correlation constant
C_d	discharge coefficient
d	injection hole diameter
l	injection hole length
$\bar{m}$	time-averaged blowing ratio, $\rho_c\bar{u}_c/\rho_\infty\bar{u}_\infty$
n	pulsation frequency
$\dot{q}''_o$	surface heat flux with no film cooling
$\dot{q}''$	spanwise-averaged surface heat flux with film cooling
Re_d	coolant Reynolds number, $d\bar{u}_c/v$
Re	freestream Reynolds number, $X\bar{u}_\infty/v$
Sr_c	injectant Strouhal number, $2\pi nl/\bar{u}_c$
Sr_∞	free-stream Strouhal number, $2\pi n\delta/\bar{u}_\infty$
Sr_x	modified Strouhal number, $Sr_c/\bar{m}^{0.6}\,(l/d)^{2.0}$
St_f	local iso-energetic Stanton number
$\overline{St_f}$	spanwise-averaged iso-energetic Stanton number
St_o	baseline Stanton number with no pulsations and no film cooling
T	temperature
$\bar{T}$	spanwise-averaged temperature
$\bar{u}_\infty$	time-averaged freestream velocity
$\bar{u}_c$	time-averaged and spatially-averaged injectant velocity
x	streamwise coordinate measured from downstream edge of film cooling holes
X	streamwise coordinate measured from boundary layer trip
z	spanwise coordinate measured from spanwise centerline of test surface.

Greek symbols

η	local film cooling effectiveness, $(T_{aw}-T_\infty)/(T_c-T_\infty)$
$\bar{\eta}$	spanwise-averaged film cooling effectiveness, $(\overline{T_{aw}}-T_\infty)/(T_c-T_\infty)$
ρ	density
θ	dimensionless coolant temperature, $(T_c-T_\infty)/(T_w-T_\infty)$
δ	boundary layer thickness
ν	kinematic viscosity.

Subscripts

aw	adiabatic wall value
c	injectant or coolant at exit planes of holes
i	ideal value
∞	freestream
w	wall value.

influences of shock waves and/or potential flow interactions on film cooling. In one of these investigations [5], time-averaged magnitudes of unsteady surface heat flux are predicted on the pressure surface of a rotor blade which are 230% greater than steady-state predictions. These are attributed to reductions of adiabatic film effectiveness by as much as 64%.

Another recent study includes flow visualization results obtained downstream of round, simple angle $l/d = 4$ film cooling holes over a range of blowing ratios when bulk flow pulsations are imposed. Two distinct types of injectant flow behavior are observed, quasi-steady, and non-quasi-steady, which are separated by magnitudes of Sr_c less than or greater than 1–2 [7]. Quasi-steady film distributions are the same as the steady distributions which would exist at the same instantaneous flow conditions. With non-quasi-steady film behavior, multiple pulsations are imposed on the injectant over the time period required for it to pass through a film hole, and alterations to time-averaged film effectiveness and film cooled boundary layer structure are often larger than when quasi-steady behavior is present [7–10]. Other recent investigations examine the effects of bulk flow pulsations on film cooling from two rows as holes [11], from different length injection holes at different blowing ratios [12], from spanwise oriented holes [13], and from holes with compound angle orientations [14]. Of these studies, Seo et al. [12] show that bulk flow pulsations have more significant effects on film cooling either as l/d decreases, or as the time-averaged blowing ratio $\bar{m}$ decreases. These investigators indicate that the largest changes are mostly due to spreading of injectant concentrations over larger volumes compared to non-pulsation distributions.

The present study also examines the effects of variations of static pressure and streamwise velocity imposed throughout a turbulent boundary layer film cooled with a single row of simple angle film cooling holes. The experimental test conditions thus model the same modes of unsteadiness which are imposed near turbine airfoil surfaces from potential flow interactions and passing families of oblique shock waves. The hole geometries and experimental conditions employed are different from ones covered in previous investigations [7–14], and include length-to-diameter ratios of 3 and 4. These values are investigated to illustrate the changes which occur with such a small l/d change, and because similar l/d values are used in operating turbines. With these and other data from the literature [7–14], a new correlation is developed and presented giving the experimental conditions which accompany the reductions in the protection which occur as bulk

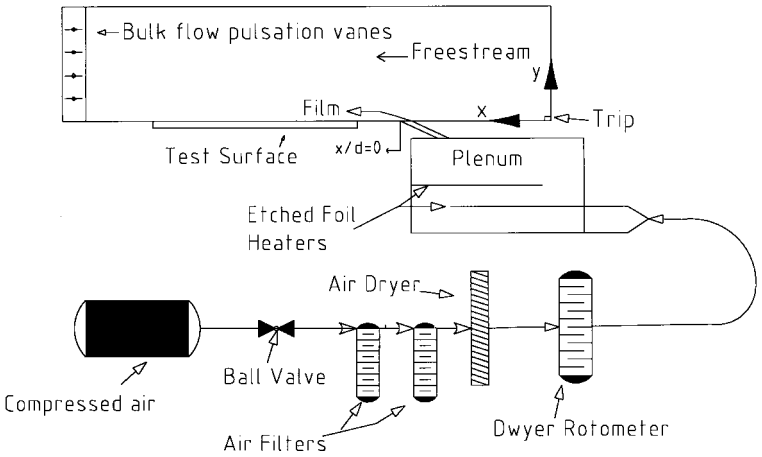

Fig. 1. Schematic diagram of experimental apparatus.

flow pulsations are imposed on film cooled boundary layers. The correlation is based on different types of experimental results [7–14], including measured distributions of adiabatic film cooling effectiveness, iso-energetic Stanton number ratio, and film cooling performance parameter given in the present paper for a variety of imposed pulsation frequencies, injectant and freestream Strouhal numbers, blowing ratios, and freestream velocities.

2. Experimental apparatus and procedures

Like a number of other recent experiments [7–14], the present experiment is also conducted on a large scale, with low speeds, flat plate test sections, and constant property flows to isolate the interactions between the film cooling, imposed bulk flow pulsations, and boundary layer.

2.1. Wind tunnel

The wind tunnel is open-circuit, subsonic, and located in the Convective Heat Transfer Laboratory of the Department of Mechanical Engineering of the University of Utah. A centrifugal blower is located at the upstream end, followed by a diffuser, a header containing a honeycomb and three screens, and then a 16:1 contraction ratio nozzle. The nozzle leads to the test section which is a rectangular duct 3.05 m long and 0.61 m wide, with a top wall having adjustable height to permit changes in the streamwise pressure gradient. The zero pressure gradient employed here is set to within 0.002 inches of water differential pressure along the length of the test section, both with and without pulsations. Flow at the test section inlet shows excellent spatial uniformity and a freestream turbulence level less than 0.1% at a freestream velocity of 10 m/s. A 5 mm high, 30 mm wide trip is placed at the beginning of the test surface to insure that the boundary layer is fully turbulent.

A schematic of the test section, including the coordinate system and film injection apparatus, is shown in Fig. 1. The downstream edge of the injection holes is 1.050 m downstream of the trip, and surface measurement stations are subsequently located at x/d of 3.87, 8.42, 15.3, 24.4, 36.6, and 42.7. Corresponding freestream Reynolds numbers, based on streamwise distance (from the trip) and a freestream velocity of 10 m/s, range from 578,000 to 1,100,000.

2.2. Film cooling injectant system

Five film cooling holes are placed in a single row with spanwise spacing of 3 hole diameters. Each hole is oriented in a streamwise/normal plane (i.e. with a simple angle orientation) at a 35° angle from the test surface. Hole diameter is 2.22 cm, giving l/d ratios of 3.0 and 4.0, and δ/d of 1.23 at $x/d=-10.7$ at a freestream velocity of 10 m/s. Ratios of displacement thickness to hole diameter, and momentum thickness to hole diameter at the same x/d and u_∞ are 0.191, and 0.136, respectively. The air used for the film first flows through a regulating ball valve, followed by an air filter and dryer system, a Dwyer rotometer, a diffuser, and finally into the injection plenum chamber. The air is cleaned and dried using a Wilkerson high capacity dryer with Wilkerson type DRP-85-060 desiccant and two coalescing filters, PSB Industries 74635-25 and Wilkerson F16-04-FO0B-C97. The regulating valve and rotometer provide means to control the film cooling flow rate, and the injection chamber provides means to heat the injectant above ambient tempera-

ture. The plenum measures 0.51 m long by 0.51 m wide with a height of 0.38 m.

Discharge coefficients are determined using an equation given by

$$C_d = \rho_c \bar{u}_c / \rho_{ci} \bar{u}_{ci} \quad (1)$$

where ρ_c is the static density at the exits of the film cooling holes, ρ_{ci} is the ideal injectant density based on plenum stagnation temperature and static pressure at the film hole exits, and $\bar{u}_{ci}$ is the ideal injectant velocity based on ρ_{ci} and the difference between plenum stagnation pressure and static pressure at the hole exits [15].

2.3. Adiabatic film cooling effectiveness measurements

Local magnitudes of the adiabatic film cooling effectiveness are deduced from measurements of coolant static temperature, freestream static temperature, and temperatures measured along an adiabatic test surface. Surface temperatures are measured at discrete locations using 150 calibrated Omega, type 5TC-TT-T-36-72, copper-constantan thermocouples, each consisting of a 36-gage wire with a soldered 2 mm diameter junction. The adiabatic surface is constructed of 101.6 mm thick of Dow Chemical Corp. Duramate Styrofoam which has a thermal conductivity of 0.027 W/m K, and a smooth plastic film layer with minimal surface imperfections placed next to the air stream. The thermocouples are oriented into six streamwise rows of twenty-five thermocouples in each row, with a spanwise spacing of 8.3 mm from $z/d = -7.5$ to $z/d = 1.5$. Each thermocouple is installed from the back of the styrofoam so that each junction is located about 0.1 mm just beneath the test surface.

Voltages produced by the thermocouples are measured and acquired using Hewlett-Packard HP44422 T thermocouple cards, installed in a Hewlett-Packard HP3497A data acquisition controller and a Hewlett-Packard HP3498A extender. The data acquisition system is connected to a Hewlett-Packard model A2240B type 362 computer used for collection and processing of data. A Pentium 200 MHz personal computer and the programs DeltaGraph 4.0, Microsoft Excel '97, and Microsoft Word '97 are used for additional processing and plotting of experimental data. As data are acquired, the injectant is heated using the etched foil heaters, with power levels controlled using a variac, to give an average plenum temperature of 50°C. Twenty-five η values for each of the six streamwise locations are averaged to determine $\bar{\eta}$ [15]. The experimental uncertainty of $\bar{\eta}$ is about $\pm 5.5\%$.

2.4. Iso-energetic Stanton number measurements

A second test surface is employed for measurements of the iso-energetic Stanton number. On the surface a thin, smooth sheet of 0.2 mm thick stainless steel foil is located next to the air stream. Copper–constantan thermocouples, 126 in number, are located directly beneath the stainless steel foil, arranged in 6 streamwise rows of 21 per row, spaced spanwise 12.7 mm apart at $z/d = 5.87$ to $z/d = -5.87$. Thermocouple wire leads are embedded in a liner under the stainless steel foil. Data reduction procedures include corrections for the temperature drop through the foil and the thermal contact resistance between the foil and the thermocouples. Directly under the liner is an Electrofilm 2.0 kilowatt model P/N 116473-2 etched foil heater encased in capton, and used to provide a constant heat flux over the surface. A 1.27-cm sheet of acrylic supports the smooth foil surface, thermocouples and foil heater. Beneath the acrylic sheet, 10.16 cm of polystyrene foam are used to insulate the surface and reduce conduction losses. All these layers are enclosed in an acrylic case and insulated with Halstead black foam insulation to further minimize conduction losses. The height of the test surface is adjustable to insure that it is flat and level next to the air stream.

For the acquisition of baseline data with no film cooling, injection holes are plugged and covered with thin plastic tape. When data are acquired either with or without film cooling, power is supplied and controlled to the foil heater using a Powerstat type 1368 variac so that the average temperature at the locations of the 126 thermocouples is 55°C. Determination of convective heat flux magnitudes requires the measurement of power to this heater, determination of gross conduction losses from the test surface, and determination of spanwise and streamwise conduction losses and gains along the steel foil. With this arrangement, an iso-energetic condition is produced wherein the freestream and injectant flows are at the same temperature. The same data acquisition and processing system (described earlier) is again used to acquire and process thermocouple voltages and other measured quantities. Twenty-one St_f/St_o values for each of the six streamwise locations are averaged to determine $\overline{St}_f/St_o$. The experimental uncertainty of $\overline{St}_f/St_o$ ranges from ± 4.0 to $\pm 6.0\%$. The experimental uncertainty of $\dot{q}''/\dot{q}''_o$ ranges from ± 3.0 to $\pm 8.0\%$. Additional details are provided by Bell [15].

3. Generation of bulk flow pulsations

Static pressure pulsations are produced in the test section using an array of rotating vanes located at the exit of the test section and driven by a system of chains, sprockets, and an electric motor, as shown in Fig. 1. Each vane is 51.0 mm wide, 3.5 mm thick, and 0.610 m long. These give pulsation velocity amplitudes

Table 1
Injectant, freestream, and pulsation experimental conditions

$\bar{u}_\infty$ (m/s)	$\bar{m}$	ρ_c/ρ_∞	$\bar{u}_c/\bar{u}_\infty$	I	l/d	n (Hz)	Sr_c ($l/d = 3$)	Sr_c ($l/d = 4$)	Sr_x ($l/d = 3$)	Sr_x ($l/d = 4$)
10	0.4	0.93	0.425	0.17	3, 4	0, 8, 20	0, 0.79, 1.97	0, 1.05, 2.63	0, 0.15, 0.38	0, 0.11, 0.28
10	0.7	0.93	0.736	0.51	3, 4	0, 8, 20	0, 0.45, 1.14	0, 0.61, 1.52	0, 0.06, 0.16	0, 0.05, 0.12
10	1.0	0.93	1.080	1.09	3, 4	0, 8, 20	0, 0.31, 0.77	0, 0.41, 1.03	0, 0.03, 0.09	0, 0.03, 0.06
4.3	1.0	0.93	1.06	1.04	3, 4	0, 8, 20	0, 0.73, 1.84	0, 0.98, 2.45	0, 0.08, 0.20	0, 0.06, 0.15

in the freestream of about $\pm 11\%$ of the time-averaged freestream velocity at $n = 20$ Hz, and about $\pm 17\%$ of the time-averaged freestream velocity at $n = 8$ Hz. The vanes are positioned so that when one vane is parallel to the test section all vanes are parallel to the test section. This approach is used because: (i) the shutters oscillate the static pressure without significant total pressure variations [16,17], (ii) static pressure pulsations produce the most important disruptions to the flow rates, trajectories, and distributions of the film coolant [7–15], (iii) much higher frequencies of pulsation can be produced than with many other methods [17], and (iv) deterministic sinusoidal variations of static pressure can be produced at selected frequencies [16].

Freestream Strouhal number $St_\infty = 2\pi n\delta/\bar{u}_\infty$ ranges from 0 to about 0.6, and gives the ratio of the boundary layer time scale to the pulsation time scale. Values greater than 1 indicate that multiple pulsations are imposed over the time interval required for first order boundary layer adjustment to a large-scale temporal change. Coolant or injectant Strouhal number $St_c = 2\pi nl/\bar{u}_c$ ranges from 0 to 2.6, compared to 0.2 to 6.0 for film cooling holes on operating turbines [10]. The coolant Strouhal number represents the ratio of the time required for the coolant to pass through the injection holes to the pulsation time scale. Values greater than 1 indicate that multiple pulsations are imposed on the film cooled boundary layer during the time required for the coolant to enter and exit the film holes [7].

4. Experimental conditions

Injectant, freestream, and pulsation experimental conditions are summarized in Table 1. The ratio of injectant to freestream density ρ_c/ρ_∞ is 0.93 for all data. Injection Reynolds number $d\bar{u}_c/v$ then ranges from 2800 to 6800. Injectant flow rates are thus always high enough to insure that turbulent flow is present at the injection hole exits without any sort of trips placed in the injection holes. Values of the modified Strouhal number Sr_x, also given in Table 1, are discussed at the end of this paper.

5. Baseline data comparisons

The present measurements downstream of $l/d = 3$ holes (with no pulsations) are compared to results from Pedersen et al. [18] and Eriksen and Goldstein [19] in Fig. 2. The spanwise-averaged adiabatic film cooling effectiveness data in Fig. 2a are obtained at about the same density ratio as the Pedersen et al. [18] data. Good agreement is seen for a time-averaged blowing ratio, $\bar{m}$, of 1.0. The present data for $\bar{m} = 0.7$ are then also in agreement since they lie between the $\bar{m} = 0.515$ and $\bar{m} = 1.05$ Pedersen et al. [18] data.

The present iso-energetic Stanton number ratio data in Fig. 2b for $\bar{m} = 1.0$ are slightly higher than the $\bar{m} = 0.99$ Eriksen and Goldstein [19] data when compared at the same x/d. When $\bar{m} = 0.7$, $\overline{St}_f/St_o$ data from the present study lie between the $\bar{m} = 0.49$ and $\bar{m} = 0.99$ data of Eriksen and Goldstein [19]. In both cases, trends and approximate magnitudes of the two

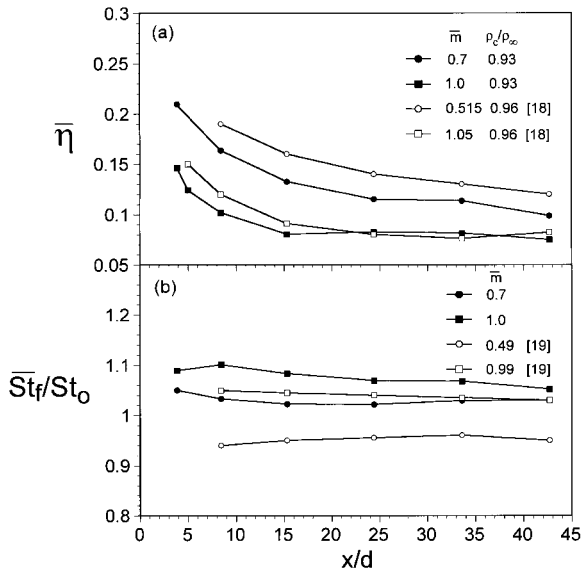

Fig. 2. Comparisons of: (a) spanwise-averaged adiabatic film cooling effectiveness distributions with measurements of Pedersen et al. [18], and (b) spanwise-averaged iso-energetic Stanton number ratios with measurements of Eriksen and Goldstein [19].

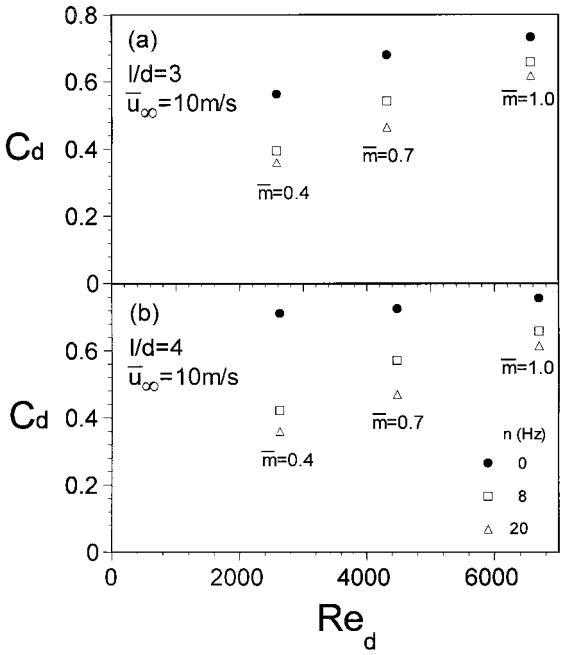

Fig. 3. Discharge coefficient variations with injectant Reynolds number at different blowing ratios and imposed pulsation frequencies, (a) $l/d = 3$, and (b) $l/d = 4$.

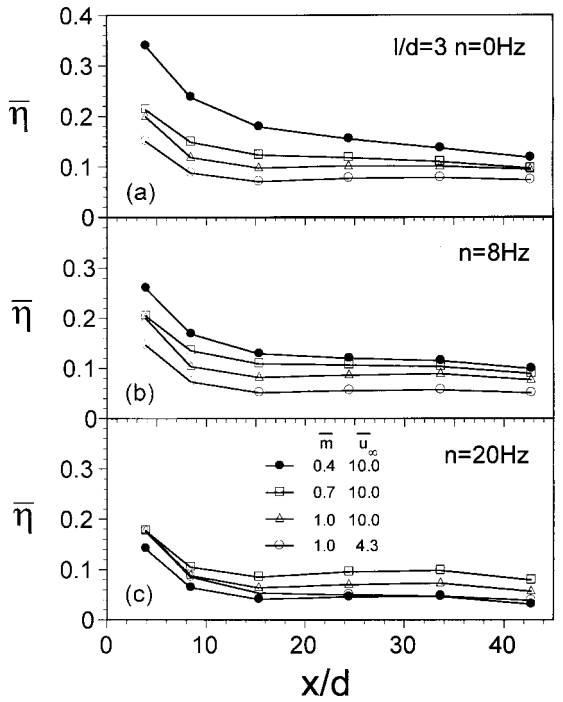

Fig. 4. Spanwise-averaged adiabatic film cooling effectiveness variations with blowing ratio and freestream velocity at different imposed pulsation frequencies for $l/d = 3$ film cooling holes, (a) $n = 0$ Hz, (b) $n = 8$ Hz, (c) $n = 20$ Hz.

$\overline{St_f}/St_o$ data sets are in rough agreement. The small differences may be due to different freestream turbulence levels or different l/d.

6. Experimental results

6.1. Discharge coefficients

Figs. 3a, b show discharge coefficients as a function of injectant hole diameter Reynolds number, Re_d, for different blowing ratios and imposed pulsation frequencies for $l/d = 3$ and $l/d = 4$ holes, respectively. As any one of these different parameters (l/d, Re_d, n) is changed, the greatest alterations to discharge coefficient magnitudes occur as the imposed pulsation frequency is altered. C_d decreases as the pulsation frequency increases when compared at the same Re_d, ρ_c/ρ_∞, $\bar{m}$, and l/d. Thus, unsteady static pressure variations (produced by the imposed pulsations) produce important changes to the injectant in the film cooling holes. Increased restrictions to film cooling flow rates result as pulsation frequency increases, especially as the separated flow region near the entrance of the hole is perturbed [12]. This is consistent with somewhat higher discharge coefficients with $l/d = 4$ holes than with the $l/d = 3$ holes. When l/d is constant and Re_d increases, changes due to varying pulsation frequency are less. The lowest C_d values are then present when Re_d is near 3000 and $n = 20$ Hz for both l/d examined.

6.2. Adiabatic film cooling effectiveness

Figs. 4 and 5 show the variation of spanwise-averaged adiabatic film cooling effectiveness with streamwise development downstream of holes with $l/d = 3$ and $l/d = 4$, respectively. Each figure is divided into three parts, corresponding to imposed pulsation frequencies of 0 Hz, 8 Hz, and 20 Hz to show changes due to varying $\bar{m}$ and $\bar{u}_\infty$ at different imposed pulsation frequencies.

Figs. 4 and 5 show that the highest effectiveness values at each x/d are obtained with no pulsations at $\bar{u}_\infty = 10$ m/s and $\bar{m} = 0.4$ for both l/d. With and without imposed pulsations, $\bar{\eta}$ values generally decrease as blowing ratio increases at each x/d. $\bar{\eta}$ values also generally decrease when the blowing ratio is held constant at $\bar{m} = 1.0$ and $\bar{u}_\infty$ decreases from 10 to 4.3 m/s. Comparing the three parts of either Fig. 4 or Fig. 5 shows that changes due to altering $\bar{m}$ of $\bar{u}_\infty$ are much smaller with $n = 20$ Hz than with $n = 0$ Hz. Thus, adiabatic effectiveness values seem to be uniformly suppressed regardless of $\bar{m}$ or $\bar{u}_\infty$ when pulsations are imposed at higher frequencies. Figs. 4 and 5 addition-

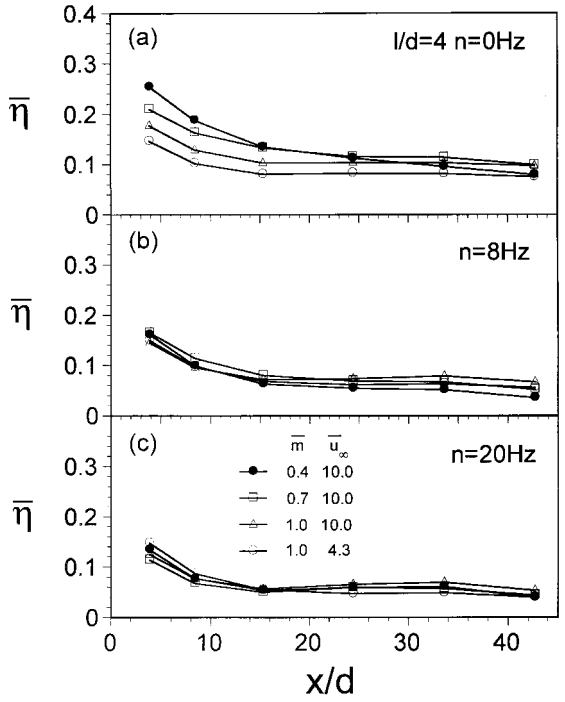

Fig. 5. Spanwise-averaged adiabatic film cooling effectiveness variations with blowing ratio and freestream velocity at different imposed pulsation frequencies for $l/d = 4$ film cooling holes, (a) $n = 0$ Hz, (b) $n = 8$ Hz, (c) $n = 20$ Hz.

ally show that $\bar{\eta}$ values generally differ more at lower x/d locations as $\bar{m}$ or $\bar{u}_\infty$ changes when considered at particular n and x/d. Exceptions occur at $n = 8$ Hz, $l/d = 4$, and at $n = 20$ Hz for both l/d since effectiveness values either increase or show only very small changes due to increases in $\bar{m}$ or decreases in $\bar{u}_\infty$.

Fig. 6 presents spanwise-averaged adiabatic film cooling effectiveness variations with normalized streamwise distance as dependent upon n and l/d for time-averaged blowing ratios of 0.4, 0.7, and 1.0 (the last $\bar{m}$ data are given for two values of $\bar{u}_\infty$). The present results for $\bar{m} = 1.0$, $l/d = 4$, and n of 0 Hz and 20 Hz are in good agreement with spanwise-averaged measurements presented by Seo et al. [12] for $\bar{m} = 1.0$, $l/d = 4$, and n of 0 and 32 Hz, respectively. When no imposed pulsations are present and $\bar{m}$ is 0.7 or 1.0, effectiveness changes negligibly in Fig. 6 due to l/d or increases slightly as l/d increases from 3 to 4. When $\bar{m} = 0.4$, effectiveness values are significantly higher at each x/d when $l/d = 3$ than when $l/d = 4$. As pulsation frequency increases, magnitudes of spanwise-averaged adiabatic film cooling effectiveness decrease when compared at the same $\bar{u}_\infty$, $\bar{m}$, x/d, and l/d. Larger changes due to pulsation frequency are present at lower blowing ratios decreases, with somewhat different quantitative changes at each $\bar{m}$ for the two l/d investigated.

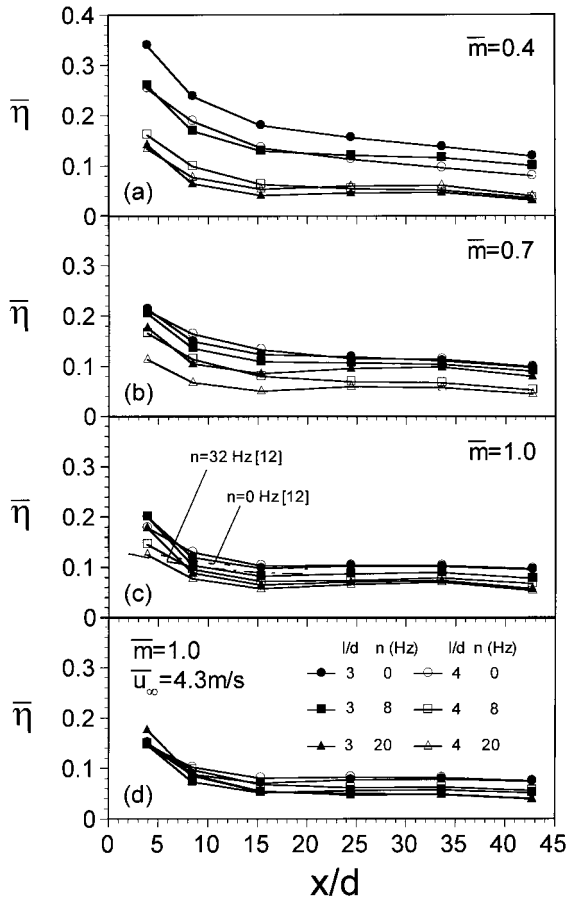

Fig. 6. Spanwise-averaged adiabatic film cooling effectiveness variations with l/d and imposed pulsation frequency n at different blowing ratios and different freestream velocities, (a) $\bar{m} = 0.4$, $\bar{u}_\infty = 10$ m/s; (b) $\bar{m} = 0.7$, $\bar{u}_\infty = 10$ m/s; (c) $\bar{m} = 1.0$, $\bar{u}_\infty = 10$ m/s; (d) $\bar{m} = 1.0$, $\bar{u}_\infty = 4.3$ m/s.

Thus, the pulsations generally have smaller influences when the film is partially or completely lifted off the test surface. At a pulsation frequency of 20 Hz, the injectant is non-quasi-steady [7]. With this behavior, the whole film trajectory lifts off the test surface in a wavy trajectory at $\bar{m}$ greater than 0.7, which allows the freestream air to move beneath the injectant in a periodic manner. As a result, corresponding film effectiveness values in Fig. 6 are reduced considerably compared to film cooled boundary layers with no pulsations.

6.3. Iso-energetic Stanton number ratios

Figs. 7 and 8 present spanwise-averaged iso-energetic Stanton number ratios as a function of x/d for $l/d = 3$ and $l/d = 4$, respectively. Variations with $\bar{m}$ and $\bar{u}_\infty$ are evident at a particular value of x/d as pulsations

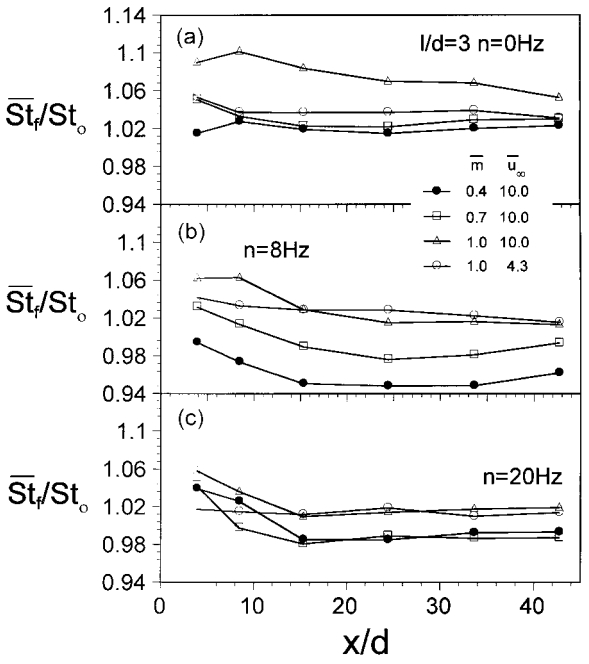

Fig. 7. Spanwise-averaged iso-energetic Stanton number ratio variations with blowing ratio and freestream velocity at different imposed pulsation frequencies for $l/d = 3$ film cooling holes, (a) $n = 0$ Hz, (b) $n = 8$ Hz, (c) $n = 20$ Hz.

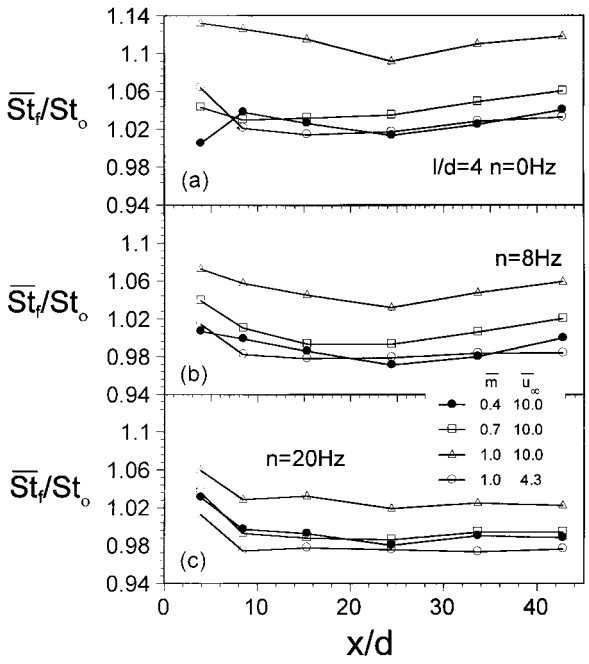

Fig. 8. Spanwise-averaged iso-energetic Stanton number ratio variations with blowing ratio and freestream velocity at different imposed pulsation frequencies for $l/d = 4$ film cooling holes, (a) $n = 0$ Hz, (b) $n = 8$ Hz, (c) $n = 20$ Hz.

are imposed at 0, 8, and 20 Hz. At $n = 0$ Hz, $\overline{St}_f/St_o$ values are greater than 1.0 for all $\bar{m}$ and $\bar{u}_\infty$ at both l/d. Generally, the highest $\overline{St}_f/St_o$ are achieved at $\bar{u}_\infty = 10$ m/s and $\bar{m} = 1.0$ for all frequencies at both l/d. These figures also show that $\overline{St}_f/St_o$ generally increases as $\bar{m}$ increases from 0.4 to 1.0 for all pulsation frequencies as $\bar{u}_\infty$ is constant at 10 m/s. With $\bar{m}$ constant at 1.0 and $\bar{u}_\infty$ changing from 4.3 to 10 m/s, the higher velocity generally gives higher $\overline{St}_f/St_o$. Exceptions occur in Fig. 7 at $n = 8$ Hz and $n = 20$ Hz, where higher $\overline{St}_f/St_o$ are sometimes present when $\bar{u}_\infty = 4.3$ m/s for x/d from 15 to 45.

Comparing Figs. 7 and 8 shows that changes also occur as l/d is changed from 3 to 4. In particular, magnitudes of $\overline{St}_f/St_o$ show changes as both l/d and $\bar{u}_\infty$ are altered. When pulsations are imposed and $l/d = 3$, $\overline{St}_f/St_o$ values in Fig. 7 for $\bar{m} = 1.0$ and $\bar{u}_\infty = 4.3$ m/s are closest to values measured when $\bar{m} = 1.0$ and $\bar{u}_\infty = 10$ m/s. In contrast, when $l/d = 4$, the $\bar{m} = 1.0$ and $\bar{u}_\infty = 4.3$ m/s data in Fig. 8 are closest to values measured when $\bar{m} = 0.4$ and $\bar{u}_\infty = 10$ m/s.

Local Stanton number ratio variations with z/d are presented in Fig. 9 for $\bar{u}_\infty = 10$ m/s and $\bar{m} = 0.7$. The most important feature of this Figure is the spanwise periodicity of the data measured at $n = 0$ Hz, which is qualitatively similar to the periodicity measured when pulsations are imposed at 8 Hz. In both cases, the $\overline{St}_f/St_o$ variations with z/d become more pronounced as the film cooled boundary layers advect downstream.

Fig. 10 illustrates the influences of imposed pulsation frequency and l/d on spanwise-averaged iso-energetic

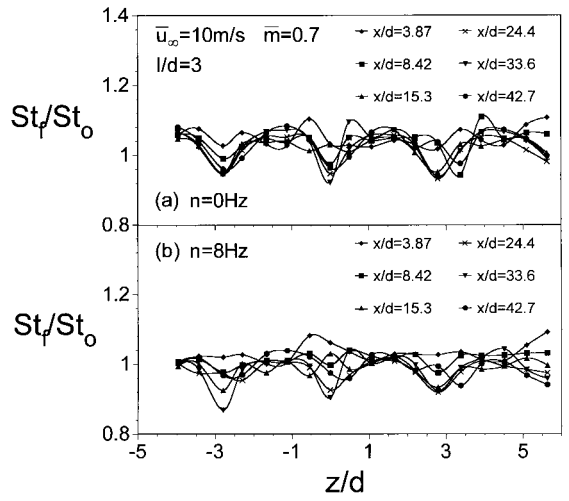

Fig. 9. Local iso-energetic Stanton number ratio variations with streamwise development for $\bar{u}_\infty = 10$ m/s, and $\bar{m} = 0.7$, (a) with no imposed pulsations, $n = 0$ Hz, and (b) with imposed pulsations, $n = 8$ Hz.

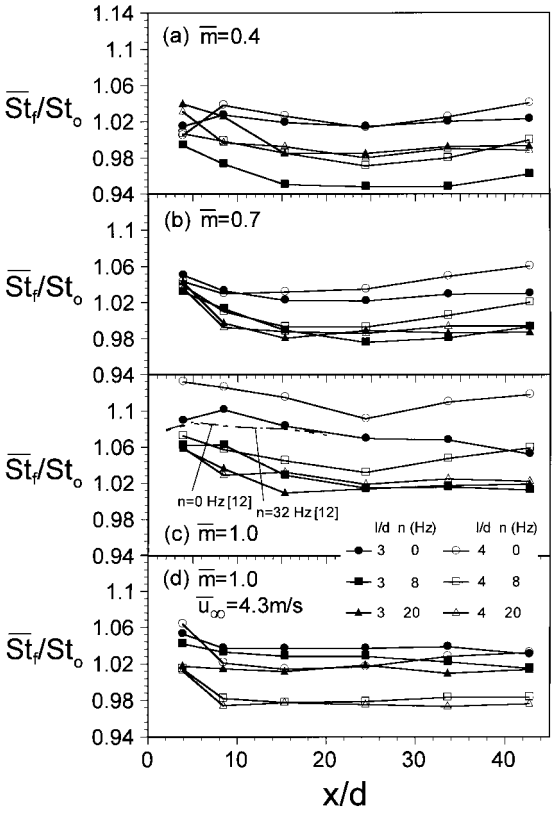

Fig. 10. Spanwise-averaged iso-energetic Stanton number ratio variations with l/d and imposed pulsation frequency n at different blowing ratios and different freestream velocities, (a) $\bar{m}=0.4$, $\bar{u}_\infty=10$ m/s; (b) $\bar{m}=0.7$, $\bar{u}_\infty=10$ m/s; (c) $\bar{m}=1.0$, $\bar{u}_\infty=10$ m/s; (d) $\bar{m}=1.0$, $\bar{u}_\infty=4.3$ m/s.

Stanton number ratios at different blowing ratios and freestream velocities. Results for $\bar{m}=1.0$, $l/d=4$, $n=0$ Hz, and $n=20$ Hz are compared with similar data given by Seo et al. [12] for $\bar{m}=1.0$, $l/d=4$, $n=0$ Hz and $n=32$ Hz, respectively. The present data show a larger change with n than the Seo et al. [12] data at this $\bar{m}$. Fig. 10 additionally shows that $\overline{St}_f/St_o$ generally decreases as pulsations are imposed at either frequency. That is, $\overline{St}_f/St_o$ generally decreases either as n increases from 0 to 8 Hz, or as n increases from 0 to 20 Hz (but not necessarily as n increases from 8 to 20 Hz). For given $\bar{u}_\infty$, l/d, and $\bar{m}$, the pulsations are thus beneficial since they result in lower $\overline{St}_f/St_o$ magnitudes (compared to values measured with no pulsations) when compared at particular values of x/d. For $\bar{u}_\infty=10$ m/s at $\bar{m}=0.4$, 0.7 and 1.0, $l/d=4$ holes generally give about the same or higher $\overline{St}_f/St_o$ than $l/d=3$ holes at each pulsation frequency and x/d location downstream.

6.4. Overall film cooling performance parameter

Figs. 11 and 12 present magnitudes of the overall film cooling performance parameter, $\dot{q}''/\dot{q}''_o$, as dependent upon x/d for $l/d=3$ and $l/d=4$, respectively. Variations with $\bar{m}$ and $\bar{u}_\infty$ are evident as pulsations are imposed at 0, 8, and 20 Hz. Magnitudes of $\dot{q}''/\dot{q}''_o$, are determined using $\theta=1.75$ in the equation $\dot{q}''/\dot{q}''_o = (\overline{St}_f/St_o)[1-\bar{\eta}\,\theta]$.

Figs. 11 and 12 show that the protection is degraded and that $\dot{q}''/\dot{q}''_o$ generally increases as $\bar{m}$ increases (as x/d, l/d, n, and $\bar{u}_\infty$ are held constant). Changes of protection with different $\bar{u}_\infty$ (for $\bar{m}=1.0$) vary somewhat with l/d and imposed pulsation frequency n. At most of the experimental conditions investigated, the best protection is then provided when the time-averaged blowing ratio $\bar{m}$ is 0.4 (through the level of protection provided by $\bar{m}=0.4$ is also achieved at other blowing ratios when $l/d=4$). The most important exception occurs when $l/d=3$ and $n=20$ Hz, wherein the lowest $\dot{q}''/\dot{q}''_o$ values are measured with $\bar{u}_\infty=10$ m/s, $\bar{m}=0.7$.

Comparing Figs. 11 and 12 reveals important influences of the length-to-diameter ratio when pulsations are imposed; $\dot{q}''/\dot{q}''_o$ differences in these two figures also further illustrate the rational for selection of these two l/d values for investigation. In the latter figure, changes due to different blowing ratios and freestream vel-

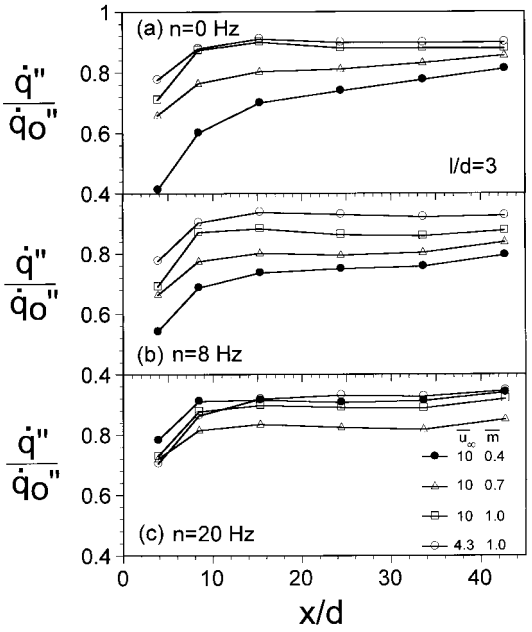

Fig. 11. Spanwise-averaged film cooling performance parameter variations with blowing ratio and freestream velocity at different imposed pulsation frequencies for $l/d=3$ film cooling holes, (a) $n=0$ Hz, (b) $n=8$ Hz, (c) $n=20$ Hz.

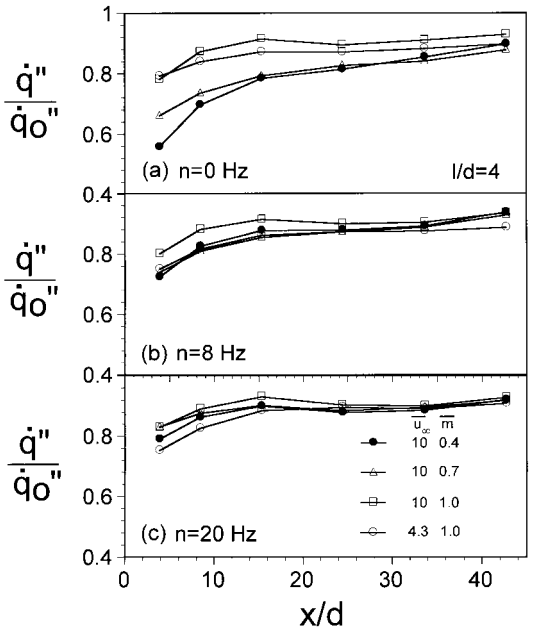

Fig. 12. Spanwise-averaged film cooling performance parameter variations with blowing ratio and freestream velocity at different imposed pulsation frequencies for $l/d = 4$ film cooling holes, (a) $n = 0$ Hz, (b) $n = 8$ Hz, (c) $n = 20$ Hz.

ocities are quite small (at all x/d investigated) as pulsations are imposed at frequencies of 8 and 20 Hz. With the same imposed frequencies, variations of $\dot{q}''/\dot{q}_o''$ due to different $\bar{m}$ and $\bar{u}_\infty$ are then much more significant in Fig. 11 for $l/d = 3$. Thus, important changes to film cooling protection occur when pulsations are present as l/d changes from 3 to 4.

Fig. 13 shows the influences of l/d and imposed pulsation frequency n on the overall film cooling performance parameter at different blowing ratios and freestream velocities. The present results for $\bar{m} = 1.0$, $l/d = 4$, $n = 0$ Hz, and $n = 20$ Hz compare favorably with data from Seo et al. [12] for the same $\bar{m}$, the same l/d, $n = 0$ Hz and $n = 32$ Hz (for x/d from 0 to 20). The largest $\dot{q}''/\dot{q}_o''$ changes with imposed pulsation frequency and length-to-diameter ratio in Fig. 13 occur at $\bar{m} = 0.4$ and $\bar{u}_\infty = 10$ m/s. At this experimental condition, protection degrades at each x/d as imposed pulsation frequency increases. Important variations with l/d are again apparent. With $l/d = 3$ holes (at $\bar{m} = 0.4$ and $\bar{u}_\infty = 10$ m/s), a dramatic increase in $\dot{q}''/\dot{q}_o''$ values occurs as n increases from 8 to 20 Hz. With $l/d = 4$ holes (at the same $\bar{m}$ and $\bar{u}_\infty$), $\dot{q}''/\dot{q}_o''$ values increase significantly as n increases from 0 to 8 Hz. Such variations result because film concentrations and film trajectories move to and from the wall with each imposed bulk flow pulsation because of instantaneous changes to the film flow rate and momentum at the

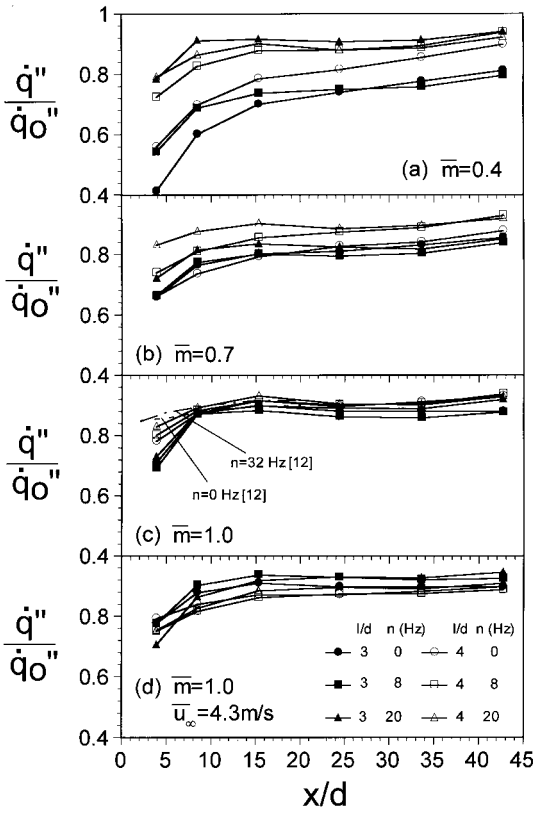

Fig. 13. Spanwise-averaged film cooling performance parameter variations with l/d and imposed pulsation velocity n at different blowing ratios and different freestream velocities, (a) $\bar{m} = 0.4$, $\bar{u}_\infty = 10$ m/s; (b) $\bar{m} = 0.7$, $\bar{u}_\infty = 10$ m/s; (c) $\bar{m} = 1.0$, $\bar{u}_\infty = 10$ m/s; (d) $\bar{m} = 1.0$, $\bar{u}_\infty = 4.3$ m/s.

cooling hole exits [7]. These then act to alter the time-averaged position of the film and mean-injectant trajectory as the pulsations act to spread the same amount of injectant over a larger volume [7,12].

Fig. 13 also shows that smaller $\dot{q}''/\dot{q}_o''$ changes with n are generally present as the blowing ratio increases to 1.0. This is because the imposed bulk flow pulsations have smaller influence on the film when it is lifted-off and its trajectory is significantly above the test surface. Comparing the $\bar{m} = 1.0$ results for $\bar{u}_\infty = 10$ m/s and $\bar{u}_\infty = 4.3$ m/s shows slightly greater variations with l/d and n at the smaller freestream velocity.

7. Summary and conclusions

Bulk flow pulsations, in the form of sinusoidal variations of static pressure and streamwise velocity, are shown to have important influences on film cooling from round, simple angle holes in a turbulent boundary layer. Distributions of adiabatic film cooling effec-

tiveness $\bar{\eta}$, iso-energetic Stanton number ratio $\overline{St}_f/St_o$, overall film cooling performance parameter $\dot{q}''/\dot{q}''_o$, and discharge coefficients C_d are all altered by the pulsations. Important reductions to the protection nominally provided by the film cooling occur as imposed pulsation frequency n increases, blowing ratio $\bar{m}$ decreases, hole length-to-diameter ratio l/d decreases, or freestream velocity $\bar{u}_\infty$ decreases. The parameter whose changes have the largest effect is n, followed by $\bar{m}$, l/d, and $\bar{u}_\infty$ (which has only a very small influence). Investigated are $\bar{u}_\infty$ of 10 and 4.3 m/s, $\bar{m}$ of 0.4, 0.7 and 1.0, l/d of 3 and 4, n equal to 0, 8, and 20 Hz, and $\rho_c/\rho_\infty = 0.93$. Ranges of other parameters are: $Re_d = 2800$–6800, Re = 578,000–1,100,000, $Sr_c = 0$–2.6, and $Sr_\infty = 0$–0.6.

The reductions in protection which occur as pulsations are imposed on film cooled boundary layers are present when

$$Sr_x = Sr_c/\bar{m}^{0.6}(l/d)^{2.0} > C_1 \tag{2}$$

where $C_1 = 0.1$–0.2, and where Sr_x can be thought of as a modified Strouhal number. Magnitudes of Sr_x are given in Table 1. Eq. (2) may be rearranged to become

$$Sr_c > C_1\bar{m}^{0.6}(l/d)^{2.0} \tag{3}$$

Correlating Eqs. (2) and (3) not only provide a good match to the present experimental data, but they are also entirely consistent with results given by Ligrani et al. [7–10], Jung and Lee [13], Jung [14], and Seo et al. [12] for l/d of 1.6, 4, and 10. Values thus also match the experimental conditions where the change from quasi-steady to non-quasi-steady behavior occurs at $Sr_c = 1.0$–2.0, $\bar{m} = 0.5$, and $l/d = 4$ [7].

According to this correlation and the data presented, alterations of the imposed pulsation frequency n and l/d have the greatest effect when the time-averaged blowing ratio $\bar{m}$ is 0.4. At this experimental condition, protection degrades, $\dot{q}''/\dot{q}''_o$ increases, $\bar{\eta}$ decreases, and $\overline{St}_f/St_o$ decreases at each x/d as imposed pulsation frequency increases. Here, decreases of $\overline{St}_f/St_o$ are beneficial since they result in better overall protection. When considered at particular values of the imposed pulsation frequency, changes to film cooling performance are generally somewhat greater when $l/d = 3$ compared to $l/d = 4$.

Discharge coefficients also decrease by important amounts as the pulsation frequency increases when compared at the same Re_d, ρ_c/ρ_∞, $\bar{m}$, and l/d.

Acknowledgements

This effort is sponsored by the National Science Foundation, Grant number CTS-9615196. Professor J. S. Lee and Dr I.-S. Jung are acknowledged for useful discussions on the research.

References

[1] M.J. Rigby, A.B. Johnson, M.L.G. Oldfield, Gas turbine rotor blade film cooling with and without simulated NGV shock waves and wakes, in: International Gas Turbine and Aeroengine Congress and Exposition, Paper No. 90-GT-78, Brussels, 1990.

[2] R.S. Abhari, A.H. Epstein, An experimental study of film cooling in a rotating transonic turbine, ASME Transactions—J. Turbomachinery 116 (1994) 63–70.

[3] K.A. Juhany, M.L. Hunt, Flowfield measurements in supersonic film cooling including effect of shock-wave interaction, AIAA Journal 32 (1994) 578–585.

[4] T. Kanda, F. Ono, M. Takahashi, T. Saito, Y. Wakamatsu, Experimental studies of supersonic film cooling with shock wave interaction, AIAA Journal 34 (1996) 265–271.

[5] R.S. Abhari, Impact of rotor-stator interaction on turbine blade film cooling, ASME Transactions—J. Turbomachinery 118 (1996) 103–113.

[6] V.K. Garg, R.S. Abhari, Comparison of predicted and experimental Nusselt number for a film-cooled rotating blade, in: International Gas Turbine and Aeroengine Congress and Exposition, Paper No. 96-GT-223, Birmingham, 1996.

[7] P.M. Ligrani, R. Gong, J.M. Cuthrell, J.S. Lee, Bulk flow pulsations and film cooling—1: injectant behavior, Int. J. Heat and Mass Transfer 39 (1996) 2271–2282.

[8] P.M. Ligrani, R. Gong, J.M. Cuthrell, J.S. Lee, Bulk flow pulsations and film cooling—2: flow structure and film effectiveness, Int. J. Heat and Mass Transfer 39 (1996) 2283–2292.

[9] P.M. Ligrani, R. Gong, J.M. Cuthrell, Bulk flow pulsations and film cooling: flow structure just downstream of the holes, ASME Transactions—J. Turbomachinery 119 (1997) 568–573.

[10] P.M. Ligrani, R. Gong, J.M. Cuthrell, J.S. Lee, Effects of bulk flow pulsations and film-cooled boundary layer structure, ASME Transactions—J. Fluids Engineering 119 (1997) 56–66.

[11] D.K. Sohn, J.S. Lee, The effects of bulk flow pulsations on film cooling from two rows of holes, in: International Gas Turbine and Aeroengine Congress and Exposition, Paper No. 97-GT-129, Orlando, 1997.

[12] H.J. Seo, J.S. Lee, P.M. Ligrani, Effects of bulk flow pulsations on film cooling from different length injection holes at different blowing ratios, in: International Gas Turbine and Aeroengine Congress and Exposition, Paper No. 98-GT-192, Stockholm, 1998.

[13] I.-S. Jung, J.S. Lee, Effects of bulk flow pulsations on film cooling from spanwise oriented holes, in: International Gas Turbine and Aeroengine Congress and Exposition, Paper No. 98-GT-211, Stockholm, 1998.

[14] I.-S. Jung, Effects of bulk flow pulsations on film cooling with compound angle injection holes, Ph.D. Thesis, Seoul National University, Seoul, S. Korea, 1998.

[15] C.M. Bell, Effects of bulk flow pulsations on film cooling with different density ratios, M.S. Thesis, University of Utah, Salt Lake City, UT, 1998.
[16] K. Al-Asmi, I.P. Castro, Production of oscillatory flow in wind tunnels, Experiments in Fluids 15 (1993) 33–41.
[17] S.K. Karlsson, An unsteady turbulent boundary layer, J. Fluid Mechanics 14 (1959) 622–636.
[18] D.R. Pedersen, E.R.G. Eckert, R.J. Goldstein, Film cooling with large density differences between the mainstream and the secondary fluid measured by the heat-mass transfer analogy, ASME Transactions—J. Heat Transfer 99 (1977) 620–627.
[19] V.L. Eriksen, R.J. Goldstein, Heat transfer and film cooling following injection through inclined circular holes, ASME Transactions—J. Heat Transfer 96 (1974) 239–245.